Series metal–organic frameworks constructed from 1,10-phenanthroline and 3,3′,4,4′-biphenyltetracarboxylic acid: Hydrothermal synthesis, luminescence and photocatalytic properties

ARTICLE *in* JOURNAL OF MOLECULAR STRUCTURE · JANUARY 2015

Impact Factor: 1.6 · DOI: 10.1016/j.molstruc.2014.09.056

4 AUTHORS:

Chong-Chen Wang
Beijing University of Civil Engineering and A…
33 PUBLICATIONS **337** CITATIONS
SEE PROFILE

Jing Huan-Ping
Tongji University
4 PUBLICATIONS **30** CITATIONS
SEE PROFILE

Peng Wang
Beijing University of Civil Engineering and A…
741 PUBLICATIONS **17,608** CITATIONS
SEE PROFILE

Shi-Jie Gao
Beijing University of Civil Engineering and A…
11 PUBLICATIONS **16** CITATIONS
SEE PROFILE

Journal of Molecular Structure 1080 (2015) 44–51

Contents lists available at ScienceDirect

Journal of Molecular Structure

journal homepage: www.elsevier.com/locate/molstruc

Series metal–organic frameworks constructed from 1,10-phenanthroline and 3,3′,4,4′-biphenyltetracarboxylic acid: Hydrothermal synthesis, luminescence and photocatalytic properties

Chong-chen Wang [a,b,*], Huan-ping Jing [a,b], Peng Wang [a], Shi-jie Gao [a]

[a] Key Laboratory of Urban Stormwater System and Water Environment (Ministry of Education), Beijing University of Civil Engineering and Architecture, Beijing 100044, China
[b] Beijing Climate Change Response Research and Education Center, Beijing University of Civil Engineering and Architecture, Beijing 100044, China

HIGHLIGHTS

- Five metal–organic frameworks are potential wide gap semi-conductive materials.
- The luminescence properties and photocatalytic activities of complexes **1**–**5** have been studied.
- Complexes **2** and **5** can be used as photocatalysts to degrade organic dye under UV light irradiation.

GRAPHICAL ABSTRACT

Five metal–organic frameworks constructed from 1,10-phenanthroline, 3,3′,4,4′-biphenyltetracarboxylic acid and different transitional metals.

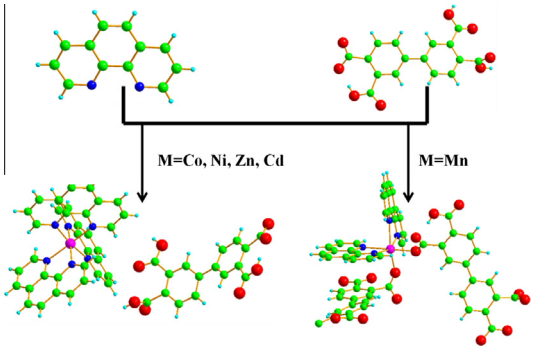

ARTICLE INFO

Article history:
Received 12 July 2014
Received in revised form 19 September 2014
Accepted 19 September 2014

Keywords:
Metal–organic framework
Luminescence
Optical energy gap
Photocatalysis
Degradation

ABSTRACT

Five novel metal–organic frameworks (MOFs) based on d^{10} metals, 1,10-phenanthroline (phen) and 3,3′,4,4′-biphenyltetracarboxylic acid (H_4bptc), namely, $[M(phen)_3(H_3bptc)_2]$ (M = Co (**1**), Ni (**2**), Zn (**3**), Cd (**4**)) and $[Mn(phen)_2(Hbptc)]\cdot 5H_2O$ (**5**) have been synthesized under hydrothermal conditions. $[M(phen)_3(H_3bptc)_2]$ consists of discrete cationic $[M(phen)_3]^{2+}$ and H_3bptc^- anion, forming 3D frameworks with the aid of hydrogen bonding and electrostatic interactions. While, the zigzag $Mn(phen)_2(Hbptc)$ chains was linked into 3D frameworks with the aid of rich hydrogen-bonding interactions. The luminescence properties and optical energy gaps of complexes **1**–**5** have been studied. In addition, complexes **2** and **5** exhibit excellent photocatalytic performance for decomposition of organic dye under UV light irradiation.

Introduction

Metal–organic frameworks (MOFs), which exhibit high surface area and large pore volume, have received great attention due to their diverse structures [1–6] and many potential applications, like

* Corresponding author at: Key Laboratory of Urban Stormwater System and Water Environment (Ministry of Education), Beijing University of Civil Engineering and Architecture, Beijing 100044, China. Tel./fax: +86 10 6832 2124.
E-mail address: chongchenwang@126.com (C.-c. Wang).

http://dx.doi.org/10.1016/j.molstruc.2014.09.056
0022-2860/

separation [7–12], gas storage [13–17], catalyst and photocatalyst [17–21], carbon dioxide capture [22–25], and so on [1–10,26–29]. Recently, much effort had also been devoted to developing new photocatalytic materials based on MOFs, which is motivated largely by a demand for solving pollution problems in view of their potential applications in the green degradation of organic pollutants [21]. An increasing number of literatures on MOFs as photocatalysts were appeared to indicate that MOFs provide a unique opportunity for integrating different molecular functional blocks to obtain good performance of organic pollutant degradation [30–34]. The continuing interest of MOFs as photocatalysts is due to the presence of organic linkers and transition metal centers, resulting in different charge-transfer transitions between ligands and metals, which make MOFs as potentially tunable photocatalysts. Additionally, MOFs usually exhibit adsorption bands in the ultraviolet region, which indicates MOFs may undergo photochemical processes and exhibit responses upon UV-light excitation [35–39].

It is well-known that the construction of MOFs is mainly dependent on the combination of several factors, such as the organic ligands, solvents, metal atoms and counter-ions. The polycarboxylate ligands, as good candidates for the construction of MOFs, have aroused a good deal of interest from chemists. 3,3′,4,4′-biphenyltetracarboxylic acid (H_4bptc) have been employed as exo-multidentate ligands for the design and construction of novel coordination polymers owing to their thermal stability and symmetry [40]. In this paper, we present five transition metal-based complexes, namely [M(phen)$_3$(H_3bptc)$_2$] (M = Co (**1**), Ni (**2**), Zn (**3**), Cd (**4**)) and [Mn(phen)$_2$(Hbptc)]·5H_2O (**5**) constructed from 1,10-phenanthroline (phen) and 3,3′,4,4′-biphenyltetracarboxylic acid (H_4bptc). The luminescent properties, optical gaps and photocatalytic activity toward methylene blue (MB) in aqueous solution were studied. The results show the promising utilization of complexes **2** and **5** for photocatalytic degradation of MB.

Experimental

All chemicals were commercially available reagent grade, and used without further purification. Elemental analyses were obtained using an Elementar Vario EL-III instrument. FTIR spectra, in the region (400–4000 cm^{-1}), were recorded on a Nicolet 6700 Fourier Transform infrared spectrophotometer. UV–Vis diffuse reflectance spectra of solid samples were measured from 200 nm to 1200 nm by Agilent Cary 5000 spectrophotometer, in which barium sulfate ($BaSO_4$) was used as the standard with 100% reflectance. Photocatalytic experiments were performed in conventional processes. A suspension containing complexes **1**–**5** (25 mg) and 50 mL MB (10 mg/L) solution was stirred under 500 W Hg lamp. A Laspec Alpha-1860 spectrometer was used to monitor the changes of the dye absorbance in the range of 400–800 nm in a 1 cm path length spectrometric quartz cell. The MB concentration was estimated by the absorbance at 664 nm.

[Co(phen)$_3$(H_3bptc)$_2$](**1**). A mixture of $CoCl_2$·6H_2O (0.3 mmol, 0.0714 g), H_4bptc (0.3 mmol, 0.0991 g) and 1,10-phen(0.6 mmol, 0.1189 g) with a molar ratio of 1:1:2 was sealed in a 25 mL Teflon-lined stainless steel Parr bomb containing deionized H_2O (20 mL), heated at 160 °C for 72 h, and then cooled down to room temperature. Light brown rod-like crystals were isolated and washed with deionized water and ethanol (yield 68% based on $CoCl_2$·6H_2O). Anal. Calcd. for **1**, $C_{68}H_{42}CoN_6O_{16}$: C, 64.9; N, 6.7; H, 3.3. Found: C, 65.0; N, 6.6; H, 3.3. IR (KBr)/cm^{-1}: 3425, 3066, 1715, 1583, 1518, 1425, 1367, 1260, 1144, 1082, 906, 849, 772, 725, 704, 641.

[Ni(phen)$_3$(H_3bptc)$_2$](**2**). Dark pink block-like crystals of **2** (yield 75% based on $NiCl_2$·6H_2O) were synthesized from a mixture of $NiCl_2$·6H_2O (0.3 mmol, 0.0713 g), H_4bptc (0.3 mmol, 0.0991 g) and 1,10-phen (0.6 mmol, 0.1189 g) with a molar ratio of 1:1:2 M ratio under the same conditions as **1**. Anal. Calcd. for **2**, $C_{68}H_{42}NiN_6O_{16}$: C, 64.9; N, 6.7; H, 3.3; H, 3.13. Found: C, 64.9; N, 6.6; H, 3.4. IR (KBr)/cm^{-1}: 3429, 3066, 2614, 2510, 1930, 1715, 1583, 1547, 1516, 1425, 1375, 1263, 1144, 1081, 906, 848, 772, 726, 704, 664, 640, 588, 539, 470, 428.

[Zn(phen)$_3$(H_3bptc)$_2$](**3**). Pink block-like crystals of **3** (yield 64% based on $ZnCl_2$) were synthesized from a mixture of $ZnCl_2$ (0.3 mmol, 0.0409 g), H_4bptc (0.3 mmol, 0.0991 g) and 1,10-phen (0.6 mmol, 0.1189 g) with a molar ratio of 1:1:2 under the same conditions as **1**. Anal. Calcd. for **3**, $C_{68}H_{42}ZnN_6O_{16}$: C, 64.5; N, 6.6; H, 3.3. Found: C, 64.6; N, 6.7; H, 3.4. IR (KBr)/cm^{-1}: 3432, 3066, 2615, 2516, 1924, 1717, 1583, 1516, 1425, 1373, 1266, 1144, 1078, 907, 849, 773, 726, 702, 640, 537, 472, 430.

[Cd(phen)$_3$(H_3bptc)$_2$](**4**). Light pink block-like crystals of **4** (yield 81% based on $CdCl_2$·2.5H_2O) were synthesized from a mixture of $CdCl_2$·2.5H_2O (0.3 mmol, 0.0684 g), H_4bptc (0.3 mmol, 0.0991 g)

Table 1
Details of X-ray data collection and refinement for complexes **1**–**5**.

	1	2	3	4	5
Formula	$C_{68}H_{42}CoN_6O_{16}$	$C_{68}H_{42}NiN_6O_{16}$	$C_{68}H_{42}ZnN_6O_{16}$	$C_{68}H_{42}CdN_6O_{16}$	$C_{40}H_{33}MnN_4O_{13}$
M	1258.01	1257.79	1264.45	1311.48	832.64
Crystal system	Monoclinic	Monoclinic	Monoclinic	Monoclinic	Monoclinic
Space group	C2/c	C2/c	C2/c	C2/c	P2(1)/c
a (Å)	28.155(2)	28.0396(12)	28.385(3)	26.768(3)	19.3369(17)
b (Å)	12.8446(5)	12.9092(3)	12.8020(11)	11.1660(9)	9.6650(8)
c (Å)	20.650(2)	20.6619(9)	20.7001(14)	22.483(2)	19.1501(18)
α (°)	90	90	90	90	90
β (°)	129.547(2)	129.749(7)	129.292(2)	122.404(2)	90.7050(10)
γ (°)	90	90	90	90	90
V (Å^3)	5758.5(8)	5750.2(4)	5821.6(8)	5673.7(9)	3578.7(5)
Z	4	4	4	4	4
μ(Mo, Kα) (mm^{-1})	0.379	0.418	0.502	0.467	0.447
Total reflections	10,851	10,909	14,504	13,928	17,445
Unique	5089	5081	5115	5007	6303
F(000)	2588	2592	2600	2672	1720
Goodness-of-fit on F^2	1.038	1.052	1.023	1.047	1.020
R_{int}	0.0283	0.0220	0.0721	0.0475	0.0632
R_0	0.0412	0.0323	0.0568	0.0427	0.0663
ωR_2	0.1000	0.0757	0.1228	0.0834	0.1720
R_1 (all data)	0.0549	0.0398	0.1518	0.0837	0.1328
ωR_2 (all data)	0.1068	0.0790	0.1759	0.1046	0.2233
Largest diff. peak and hole (e/Å^3)	0.344, −0.401	0.252, −0.355	0.349, −0.312	0.516, −0.324	0.727, −0.577

Table 2
Selected bond lengths and angles for complexes **1–5** [Å and °].

(**1**)

Bond lengths (Å)

Co(1)–N(1)#1	2.1071(17)	Co(1)–N(1)	2.1071(17)	Co(1)–N(2)	2.131(2)
Co(1)–N(2)#1	2.131(2)	Co(1)–N(3)#1	2.134(2)	Co(1)–N(3)	2.134(2)

Bond angles (°)

N(1)#1–Co(1)–N(1)	172.09(11)	N(1)#1–Co(1)–N(2)	95.28(7)
N(1)–Co(1)–N(2)	79.21(7)	N(1)#1–Co(1)–N(2)#1	79.21(7)
N(1)–Co(1)–N(2)#1	95.28(7)	N(2)–Co(1)–N(2)#1	92.73(11)
N(1)#1–Co(1)–N(3)#1	91.59(7)	N(1)–Co(1)–N(3)#1	94.52(7)
N(2)–Co(1)–N(3)#1	170.77(8)	N(2)#1–Co(1)–N(3)#1	94.60(8)
N(1)#1–Co(1)–N(3)	94.52(7)	N(1)–Co(1)–N(3)	91.59(7)
N(2)–Co(1)–N(3)	94.60(8)	N(2)#1–Co(1)–N(3)	170.77(8)
N(3)#1–Co(1)–N(3)	78.69(13)		

Symmetry transformations used to generate equivalent atoms: #1 $-x+3, y, -z+3/2$

(2)

Bond lengths (Å)

Ni(1)–N(1)#1	2.0718(14)	Ni(1)–N(1)	2.0718(14)	Ni(1)–N(2)#1	2.0853(16)
Ni(1)–N(2)	2.0853(16)	Ni(1)–N(3)#1	2.0908(17)	Ni(1)–N(3)	2.0908(17)

Bond angles (°)

N(1)#1–Ni(1)–N(1)	173.10(9)	N(1)#1–Ni(1)–N(2)#1	80.71(6)
N(1)–Ni(1)–N(2)#1	94.49(6)	N(1)#1–Ni(1)–N(2)	94.49(6)
N(1)–Ni(1)–N(2)	80.71(6)	N(2)#1–Ni(1)–N(2)	92.60(9)
N(1)#1–Ni(1)–N(3)#1	91.57(6)	N(1)–Ni(1)–N(3)#1	93.72(6)
N(2)#1–Ni(1)–N(3)#1	93.93(6)	N(2)–Ni(1)–N(3)#1	171.73(6)
N(1)#1–Ni(1)–N(3)	93.72(6)	N(1)–Ni(1)–N(3)	91.56(6)
N(2)#1–Ni(1)–N(3)	171.73(6)	N(2)–Ni(1)–N(3)	93.93(6)
N(3)#1–Ni(1)–N(3)	80.04(10)		

Symmetry transformations used to generate equivalent atoms: #1 $-x+1, y, -z+3/2$

(**3**)

Bond lengths (Å)

Zn(1)–N(1)#1	2.122(4)	Zn(1)–N(1)	2.122(4)	Zn(1)–N(2)#1	2.151(4)
Zn(1)–N(2)	2.151(4)	Zn(1)–N(3)#1	2.157(5)	Zn(1)–N(3)	2.157(5)

Bond angles (°)

N(1)#1–Zn(1)–N(1)	170.7(2)	N(1)#1–Zn(1)–N(2)#1	78.33(17)
N(1)–Zn(1)–N(2)#1	95.31(17)	N(1)#1–Zn(1)–N(2)	95.31(17)
N(1)–Zn(1)–N(2)	78.33(17)	N(2)#1–Zn(1)–N(2)	94.8(2)
N(1)#1–Zn(1)–N(3)#1	92.82(17)	N(1)–Zn(1)–N(3)#1	94.43(18)
N(2)#1–Zn(1)–N(3)#1	94.4(2)	N(2)–Zn(1)–N(3)#1	168.8(2)
N(1)#1–Zn(1)–N(3)	94.43(18)	N(1)–Zn(1)–N(3)	92.82(17)
N(2)#1–Zn(1)–N(3)	168.8(2)		

Symmetry transformations used to generate equivalent atoms: #1 $-x+1, y, -z+3/2$

(4)

Bond lengths (Å)

Cd(1)–N(1)	2.350(3)	Cd(1)–N(1)#1	2.350(3)	Cd(1)–N(3)	2.350(3)
Cd(1)–N(3)#1	2.350(3)	Cd(1)–N(2)	2.351(3)	Cd(1)–N(2)#1	2.351(3)

Bond angles (°)

N(1)–Cd(1)–N(1)#1	106.37(16)	N(1)–Cd(1)–N(3)	94.12(11)
N(1)#1–Cd(1)–N(3)	154.36(11)	N(1)–Cd(1)–N(3)#1	154.36(11)
N(1)#1–Cd(1)–N(3)#1	94.12(11)	N(3)–Cd(1)–N(3)#1	71.40(17)
N(1)–Cd(1)–N(2)	71.40(11)	N(1)#1–Cd(1)–N(2)	94.47(10)
N(3)–Cd(1)–N(2)	106.80(10)	N(3)#1–Cd(1)–N(2)	92.15(11)
N(1)–Cd(1)–N(2)#1	94.47(10)	N(1)#1–Cd(1)–N(2)#1	71.40(10)
N(3)–Cd(1)–N(2)#1	92.15(11)	N(3)#1–Cd(1)–N(2)#1	106.80(10)
N(2)–Cd(1)–N(2)#1	156.80(15)		

Symmetry transformations used to generate equivalent atoms: #1 $-x+1, y, -z+3/2$

(5)

Bond lengths (Å)

Mn(1)–O(3)	2.104(4)	Mn(1)–O(8)#1	2.165(4)	Mn(1)–N(1)	2.264(5)
Mn(1)–N(3)	2.266(5)	Mn(1)–N(2)	2.319(5)	Mn(1)–N(4)	2.319(5)

Bond angles (°)

O(3)–Mn(1)–O(8)#1	85.79(15)	O(3)–Mn(1)–N(1)	90.49(16)
O(8)#1–Mn(1)–N(1)	97.03(16)	O(3)–Mn(1)–N(3)	108.88(16)
O(8)#1–Mn(1)–N(3)	102.79(17)	N(1)–Mn(1)–N(3)	153.04(17)

Table 2 (*continued*)

O(3)–Mn(1)–N(2)	162.62(16)	O(8)#1–Mn(1)–N(2)	92.39(15)
N(1)–Mn(1)–N(2)	72.55(17)	N(3)–Mn(1)–N(2)	88.39(17)
O(3)–Mn(1)–N(4)	96.26(15)	O(8)#1–Mn(1)–N(4)	175.48(17)
N(1)–Mn(1)–N(4)	87.00(17)	N(3)–Mn(1)–N(4)	72.74(17)
N(2)–Mn(1)–N(4)	86.84(16)		

Symmetry transformations used to generate equivalent atoms: #1 $x, -y+1/2, z+1/2$; #2 $x, -y+1/2, z-1/2$

and 1,10-phen (0.6 mmol, 0.1189 g) with a molar ratio of 1:1:2 M ratio under the same conditions as **1**. Anal. Calcd. for **4**, $C_{68}H_{42}CdN_6O_{16}$: C, 62.2; N, 6.4; H, 3.2. Found: C, 62.3; N, 6.5; H, 3.3. IR (KBr)/cm^{-1}: 3440, 3055, 2611, 2507, 1939, 1713, 1584, 1547, 1516, 1425, 1367, 1262, 1144, 1098, 1045, 906, 850, 772, 726, 664, 639, 589, 470, 418.

$[Mn(phen)_2(Hbptc)]\cdot 5H_2O$(**5**). Light yellow rod-like crystals of **5** (yield 72% based on $MnCl_2\cdot 4H_2O$) were synthesized from a mixture of $MnCl_2\cdot 4H_2O$ (0.3 mmol, 0.0594 g), H_4bptc (0.3 mmol, 0.0991 g) and 1,10-phen (0.6 mmol, 0.1189 g) with a molar ratio of 1:1:2 under the same conditions as **1**. Anal. Calcd. for **5**, $C_{40}H_{33}MnN_4O_{13}$: C, 57.6; N, 6.7; H, 4.0. Found: C, 57.7; N, 6.6; H, 4.0. IR (KBr)/cm^{-1}: 3435, 3071, 2608, 1933, 1703, 1580, 1517, 1424, 1364, 1301, 1252, 1144, 1103, 1046, 913, 850, 806, 772, 728, 638, 613, 535, 439.

X-ray crystallography

X-ray single-crystal data collection for complexes **1–5** was performed with Bruker CCD area detector diffractometer with a graphite-monochromatized Mo Kα radiation ($\lambda = 0.71073$ Å) using φ–ω mode at 298(2) K. The SMART software [41] was used for data collection and the SAINT software [42] for data extraction. Empirical absorption corrections were performed with the SADABS program [43]. The structure has been solved by direct methods (SHELXS-97) [44] and refined by full-matrix-least squares techniques on F^2 with anisotropic thermal parameters for all of the non-hydrogen atoms (SHELXL-97) [44]. All hydrogen atoms were located by Fourier difference synthesis and geometrical analysis. These hydrogen atoms were allowed to ride on their respective parent atoms. All structural calculations were carried out using the SHELX-97 program package [44]. Crystallographic data and structural refinements for complexes **1–5** are summarized in Table 1. Selected bond lengths and angles for all complexes are listed in Table 2.

Results and discussion

*Structural description for **1–4***

Complexes **1–4** are isomorphous and isostructural, hence, only the structure of **1** is described in detail. The crystal structure analysis reveal that the complex **1** consists of discrete cationic $[Co(phen)_3]^{2+}$ and H_3bptc^- anion. The Co(II), in an octahedral geometry, is six-coordinated by six nitrogen atoms from three different phen ligands, in which two nitrogen atoms (N1 and N1#1) occupy the axial positions, and the remaining four nitrogen atoms (N2, N2#1, N3 and N3#1) lie in the four sites of equatorial plane, as shown in Fig. 1(a). In the equatorial plane, the bond angles of N2–Co1–N3, N2#1–Co1–N2, N3#1–Co1–N3, N3#1–Co1–N2#1 are 94.60(8)°, 95.28(7)°, 78.69(13)° and 94.60(8)°, respectively, and the bond angle of N1–Co1–N1#1 is 172.09(11)°, implying the Co-centered coordination octahedron is slightly distorted. And the dihedral angles between the three phen molecules are 84.2°,

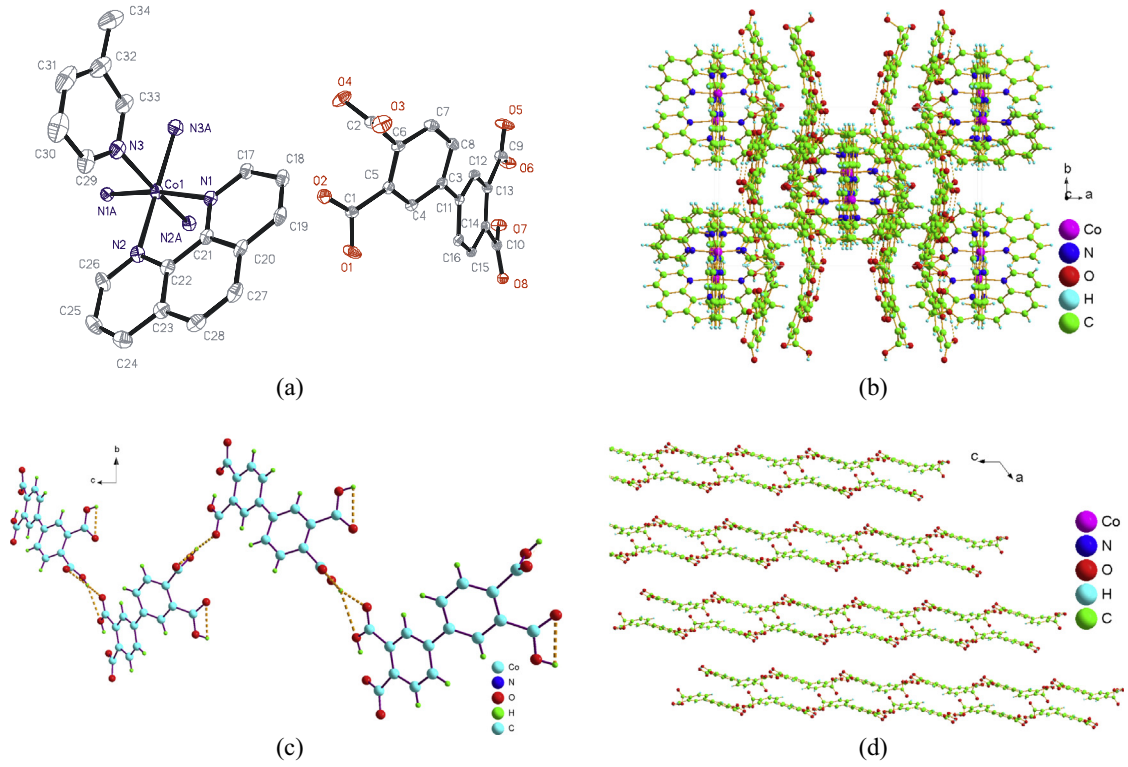

Fig. 1. (a) Asymmetric unit of $[Co(phen)_3(H_3bptc)_2]$ (**1**) and coordination environments around the Co(II) atoms. (b) Packing view of 3D framework built from $[Co(phen)_3]^{2+}$ cations and H_3bptc^- anions along the *c*-axis for complex **1**. (c) The anionic chains constructed from H_3bptc^- anions with hydrogen-bonding interactions in complex **1**. (d) 2D anionic sheet constructed from H_3bptc^- anions with the aid of hydrogen-bonding interactions.

84.3° and 89.4°, respectively. The discrete H_3bptc^- acts as counter-ion to compensate the charge of $[Co(phen)_3]^{2+}$, in which the dihedral angle between the two benzene rings (the ring of C3–C4–C5–C5–C6–C7–C8 and the ring of C11–C12–C13–C14–C15–C16) is 25.451(8)°. The partly deprotonated H_3bptc^- anions are joined into 1D chain by hydrogen-bonding interactions as shown in Fig. 1(c) and (d) and Table 3. The neighboring $[Co(phen)_3]^{2+}$ cations and H_3bptc^- anions are further joined into a 3D framework by hydrogen bonding and electrostatic interactions, as shown in Fig. 1(b).

Structural description for ***5***

In complexes **5**, the Mn center is octahedrally coordinated by O3 and N2, at the axial direction, and O8, N1, N3, N4 in the equatorial plane, in which O3 and O8 are from two different deprotonated $Hbptc^{3-}$ ligands, and N1, N2, N3 and N4 come from two different phen ligands, as depicted in Fig. 2(a) and (b). The Mn-centered coordination octahedron is distorted, with the bond lengths, 2.104(4) and 2.165(4) Å for Mn–O bonds, and 2.264(5)–2.319(5) Å for Mn–N bonds, and the bond angles deviated to 90° or 180°, as illustrated in Table 2. Phen acts as chelating ligand to join a Mn center, while the deprotonated $Hbptc^{3-}$ acts as both bis-mono dentate ligands to link two Mn centers into a zigzag $Mn(phen)_2(Hbptc)$ chain with the aid of phen ligands and counter-ion to compensate the anionic charge of the above-stated zigzag chain (Fig. 2(d)). As shown in Fig. 2(c), the adjacent $Mn(phen)_2(Hbptc)$ chains are further linked into three-dimensional framework with the aid of rich hydrogen-bonding interactions, as listed in Table 3.

Luminescence properties

Luminescent properties of complexes with d^{10} metal centers have attracted much interest due to their potential applications in electroluminescent display, chemical sensors, and photochemistry [40,45]. Therefore, in this work, the luminescent properties of H_4bptc, phen and complexes **1**–**5** have been investigated in the solid state at room temperature. The emission peaks are shown in Fig. 3. The emission spectra of free H_4bptc and phen ligands show the main peaks at 393 and 365&380 nm, respectively, which are probably attributable to the $\pi^* \rightarrow n$ or $\pi^* \rightarrow \pi$ transitions. The emission spectra of the complexes exhibit emissions at about 374 nm (λ_{ex} = 320 nm) for **1**, 393 nm (λ_{ex} = 320 nm) for **2**, 385 nm (λ_{ex} = 320 nm) for **3**, 408 nm (λ_{ex} = 320 nm) for **4** and 393 nm (λ_{ex} = 320 nm) for **5**, respectively, which are similar to that of H_4bptc. Therefore, the emission bands of complexes **1**–**5** can be attributed to the intraligand π–π^* transitions of the ligand, which is comparable to the complex constructed from H_4bptc [40].

Optical energy gap

In order to explore the conductivity of the title complexes, the measurement of diffuse reflectivity for a powder sample was used to obtain its band gap E_g. The band gap E_g was determined as the intersection point between the energy axis and the line extrapolated from the linear portion of the absorption edge in a plot of Kubelka–Munk function F against energy E. Kubelka–Munk function, $F = (1 - R)^2/2R$, was converted from the recorded diffuse reflectance data, where R is the reflectance of an infinitely thick layer at a given wavelength. The F versus E plots for the complex **1–5** are shown in Fig. 4, where steep absorption edges are displayed and the E_g of all complexes can be assessed at 3.0 eV, 3.3 eV, 3.4 eV, 3.4 eV and

Table 3
Hydrogen bonds for complexes **1**–**5** (Å and °).

D–H	d(D–H)	d(H···A)	∠DHA	d(D···A)	A
(1)					
O1–H1	0.820	1.810	159.52	2.595	O8 [x, $-y+2$, $z+1/2$]
O1–H1	0.820	2.580	116.94	3.041	O7 [x, $-y+2$, $z+1/2$]
O4–H4	0.820	1.813	166.13	2.617	O5 [x, $-y+1$, $z+1/2$]
O6–H6	0.820	1.577	175.97	2.395	O7
(2)					
O1–H1	0.820	1.807	161.56	2.598	O8 [x, $-y+2$, $z+1/2$]
O1–H1	0.820	2.608	117.28	3.071	O7 [x, $-y+2$, $z+1/2$]
O4–H4	0.820	1.817	166.71	2.622	O5 [x, $-y+1$, $z+1/2$]
O6–H6	0.820	1.582	174.79	2.400	O7
(3)					
O1–H1	0.820	1.819	166.71	2.624	O8 [x, $-y$, $z+1/2$]
O4–H4	0.820	1.823	159.47	2.607	O5 [x, $-y+1$, $z+1/2$]
O4–H4	0.820	2.568	117.39	3.033	O6 [x, $-y+1$, $z+1/2$]
O6–H6	0.820	1.625	147.66	2.359	O7
(4)					
O1–H1	0.820	1.820	168.42	2.628	O8 [x, $-y+2$, $z+1/2$]
O1–H1	0.820	2.496	131.20	3.098	O7 [x, $-y+2$, $z+1/2$]
O3–H3	0.820	1.786	150.29	2.531	O5 [x, $-y+1$, $z+1/2$]
O7–H7	0.820	1.564	170.93	2.377	O6
(5)					
O6–H6	0.820	1.658	162.18	2.451	O7
O9–H9C	0.850	1.965	150.33	2.736	O4
O9–H9D	0.850	1.937	146.19	2.685	O1 [$-x+1$, $y-1/2$, $-z+3/2$]
O10–H10C	0.850	1.934	158.71	2.743	O2
O10–H10D	0.850	2.134	134.46	2.796	O13 [$-x+1$, $y+1/2$, $-z+3/2$]
O10–H10D	0.850	2.137	158.67	2.945	O9 [$-x+1$, $y+1/2$, $-z+3/2$]
O10–H10A	0.850	2.035	153.31	2.821	O10 [$-x+1$, $-y+2$, $-z+1$]
O11–H11C	0.850	2.002	161.85	2.822	O4
O11–H11D	0.850	1.956	161.39	2.775	O9 [$-x+1$, $y-1/2$, $-z+3/2$]
O12–H12C	0.850	1.947	173.15	2.793	O5 [$x+1$, $y+1$, z]
O12–H12D	0.850	2.475	173.57	3.321	O7 [$-x+1$, $-y+1$, $-z+1$]
O13–H13C	0.850	2.178	168.45	3.015	O3
O13–H13D	0.850	1.438	168.33	2.277	O9

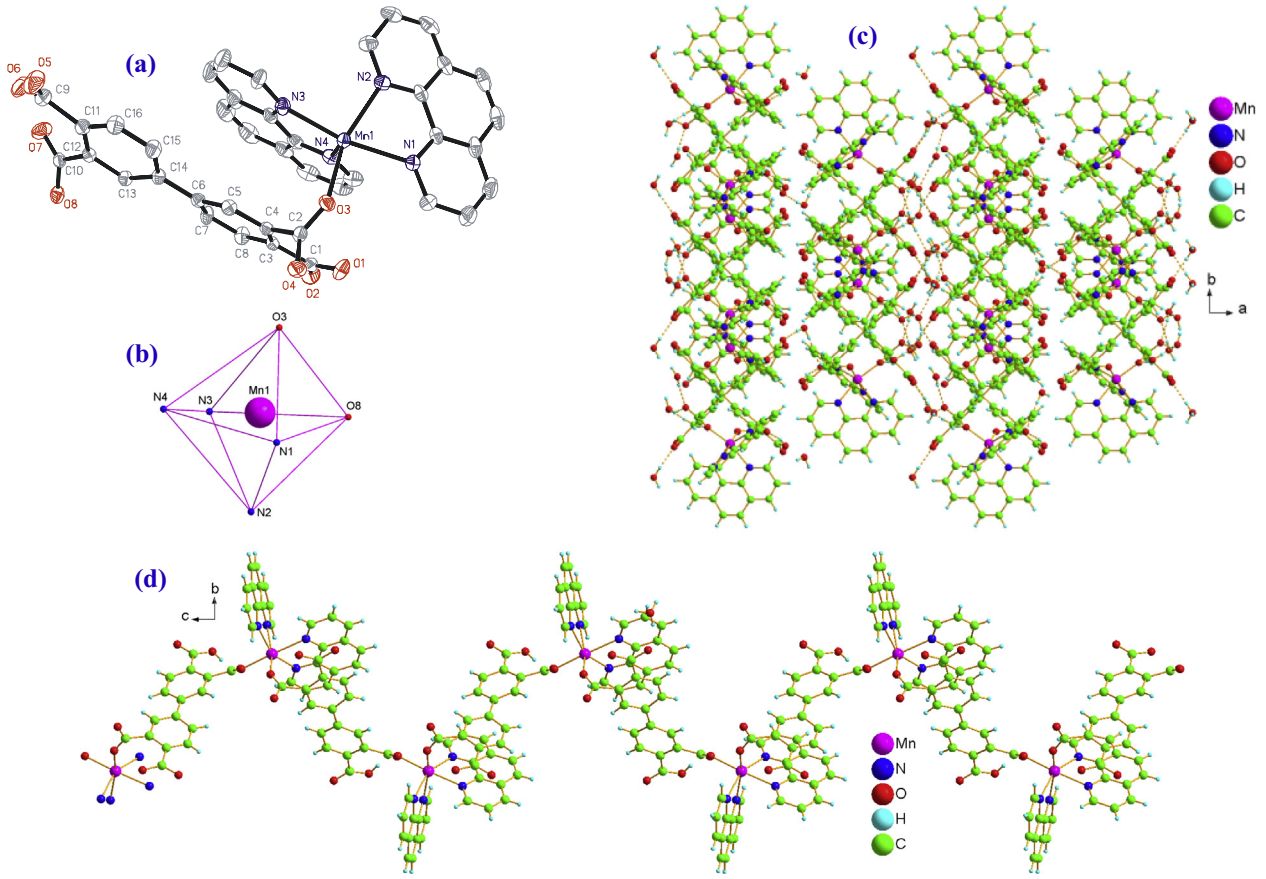

Fig. 2. (a) Asymmetric unit of $[Mn(phen)_2(Hbptc)]\cdot 5H_2O$ (**5**). (b) Highlight of the coordination polyhedra for Mn(III) ions in complex **5**. (c) Packing view of 3D framework built from $[Mn(phen)_2(Hbptc)]$ and lattice H_2O molecules with the aid of hydrogen-bonding interactions along the *c*-axis for complex **5**. (d) The Zigzag $[Mn(phen)_2(Hbptc)]$ chain in complex **5**.

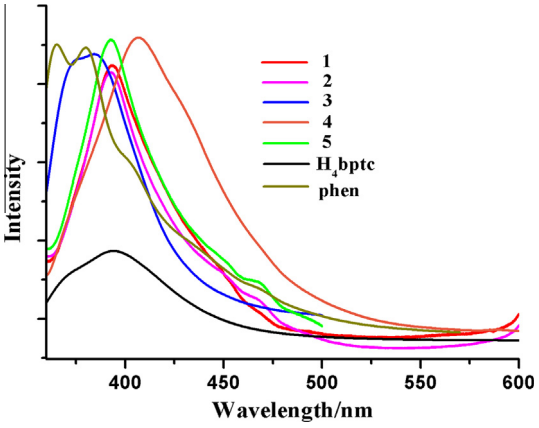

Fig. 3. Luminescent emission spectra of complexes **1–5**, free H_4bptc, and phen ligands in the solid state at room temperature.

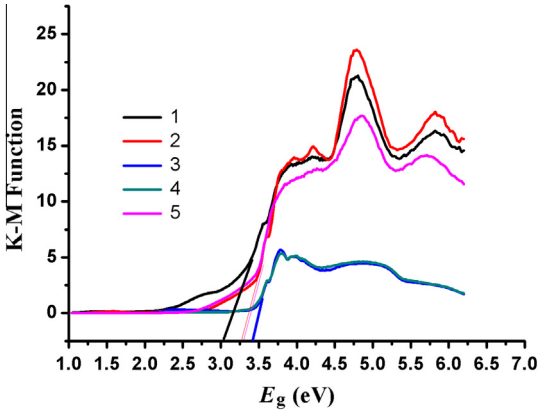

Fig. 4. Kubelka–Munk-transformed diffuse reflectance spectra of complexes **1–5**.

3.3 eV, respectively, which indicate that complexes **1–5** are potential wide gap semiconductive materials [46–49].

Photocatalytic activity

Photocatalysts have attracted much attention due to their potential applications in purifying water and air by completely decomposing organic pollutants [50]. Methylene blue (MB), as a model of dye contaminant, was selected for evaluating the activities of photocatalysts in decomposition of organic pollutants in wastewater. In addition, MB is commonly used as a representative of a type widespread organic dyes that are very difficult to be decomposed in waste streams under UV irradiation [51]. The photocatalytic performances of complexes **1–5** for the photodegradation of MB were carried out under UV irradiation. Additionally, control experiments on photodegradation of MB were performed. The concentration changes of MB (C/C_0) versus reactions times (t) of complexes **1–5** are plotted in Fig. 5. It can be seen that the photocatalytic activities increase from 20.1% (without any catalyst) to 30.9% for **1**, 84.2% for **2**, 70.1% for **3**, 55.4% for **4** and 97.6% for **5**

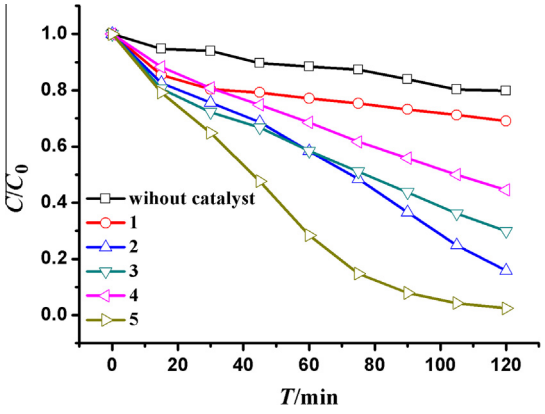

Fig. 5. Photocatalytic decomposition of MB solution under UV with the use of complexes **1**–**5**, and the control experiment without any catalyst.

after 2 h of UV light irradiation. These results revealed that complexes **2** and **5** may be potential candidates for photocatalytic degradation of MB, which is comparable with the previously reported results [15–21].

As is known, in the presence of UV light, there is an electron transfer from the highest occupied molecular orbital (HOMO) to the lowest unoccupied molecular orbital (LUMO). The HOMO is mainly contributed by O and/or N 2p bonding orbitals, and the LUMO is mainly contributed by empty M (like Mn) orbitals. Once in the presence of UV light, there was an electron transfer from the HOMO to LUMO. The electron of the excited state in the LUMO was usually very easily lost, while the HOMO strongly demanded one electron to return to its stable state. Therefore, one electron was captured from water molecules, which was oxygenated into the ·OH active species. Then, the ·OH could decompose MB efficiently to complete the photocatalytic process. A similar mechanism had been proposed recently for the degradation of organic dyes in the presence of similar metal–organic frameworks [21]. It should be pointed out that some MOFs were labeled as semiconductors based on their optical transition properties and electrochemical and photochemical activities [52–54]. But, recently Gascon and coworkers pointed out that such semiconducting behavior only occurs in a very limited subset of MOFs [55]. As to photocatalysis, MOFs should be treated as molecular catalysts rather than as typical semiconductors [55,56]. To understand the photocatalysis mechanisms of MOFs, they suggested that the terminology of HOMO–LUMO gap should be utilized to describe the discrete character of the light-induced transitions in the MOFs [55]. Therefore, it is easy to understand that only complexes **2** and **5** exhibit good photocatalytic activities, although all complexes **1**–**5** have nearly identical optical energy gaps.

Conclusions

Five new metal–organic frameworks were successfully synthesized under hydrothermal conditions through variation of d^{10} metal salts with phen and H_4bptc. Complexes **1**–**4** are isomorphous and isostructural, which consist of discrete cationic $[M(phen)_3]^{2+}$ and H_3bptc^- anion. While, in complex **5**, the deprotonated $Hbptc^{3-}$ acts as bis-mono dentate ligand to link $[Mn(phen)]^{2+}$ into zigzag chain. The emission bands of complexes **1**–**5** can be attributed to the intraligand π–π^* transitions of the H_4bptc. The optical gap complexes **1**–**5** were 3.0 eV, 3.3 eV, 3.4 eV, 3.4 eV and 3.3 eV, respectively, implying that they can be used as potential wide gap semiconductive materials. Complexes **2** and **5** exhibited efficient photocatalytic activities in degrading organic dyes (like MB in this case). Further researches should be carried out to clarify the photocatalytic activities on other organic pollutants.

Acknowledgements

We thank the financial support from the Beijing Natural Science Foundation & Scientific Research Key Program of Beijing Municipal Commission of Education (KZ201410016018), the Training Program Foundation for the Beijing Municipal Excellent Talents (2013D005017000004), the Importation & Development of High-Caliber Talents Project of Beijing Municipal Institutions (CIT&CD201404076), and China Postdoctoral Science of Foundation (2013M540831), Open Research Fund Program of Key Laboratory of Urban Stormwater System and Water Environment (Ministry of Education).

Appendix A. Supplementary material

CCDC 1012421-1012425 contain the supplementary crystallographic data for this paper. These data can be obtained free of charge from The Cambridge Crystallographic Data Centre via www.ccdc.cam.ac.uk/data_request/cif. Supplementary data associated with this article can be found, in the online version, at http://dx.doi.org/10.1016/j.molstruc.2014.09.056.

References

[1] C.C. Wang, H.Y. Li, G.L. Guo, P. Wang, Transit. Met. Chem. 38 (2013) 275.
[2] C.C. Wang, G.L. Guo, P. Wang, Transit. Met. Chem. 38 (2013) 455.
[3] C.C. Wang, G. Guo, P. Wang, J. Mol. Struct. 1032 (2012) 93.
[4] C.C. Wang, Z. Wang, F. Gu, G. Guo, J. Mol. Struct. 1004 (2011) 39.
[5] C.C. Wang, P. Wang, G.S. Guo, Transit. Met. Chem. 35 (2010) 721.
[6] C.C. Wang, Z. Wang, F. Gu, G. Guo, J. Mol. Struct. 979 (2010) 92.
[7] J.-R. Li, J. Yu, W. Lu, L.B. Sun, J. Sculley, P.B. Balbuena, H.C. Zhou, Nat. Commun. 4 (2013) 1538.
[8] J.-R. Li, J. Sculley, H.C. Zhou, Chem. Rev. 112 (2011) 869.
[9] J.-R. Li, H.C. Zhou, Nat. Chem. 2 (2010) 893.
[10] J.-R. Li, D.J. Timmons, H.C. Zhou, J. Am. Chem. Soc. 131 (2009) 6368.
[11] J.-R. Li, R.J. Kuppler, H.C. Zhou, Chem. Soc. Rev. 38 (2009) 1477.
[12] L. Pan, D.H. Olson, L.R. Ciemnolonski, R. Heddy, J. Li, Angew. Chem. 118 (2006) 632.
[13] N.L. Rosi, J. Eckert, M. Eddaoudi, D.T. Vodak, J. Kim, M. O'Keeffe, O.M. Yaghi, Science 300 (2003) 1127.
[14] J.L. Rowsell, O.M. Yaghi, Angew. Chem. Int. Ed. 44 (2005) 4670.
[15] D.J. Collins, H.C. Zhou, J. Mater. Chem. 17 (2007) 3154.
[16] S. Ma, H.C. Zhou, Chem. Commun. 46 (2010) 44.
[17] R.J. Kuppler, D.J. Timmons, Q.R. Fang, J.R. Li, T.A. Makal, M.D. Young, D. Yuan, D. Zhao, W. Zhuang, H.C. Zhou, Coord. Chem. Rev. 253 (2009) 3042.
[18] J. Lee, O.K. Farha, J. Roberts, K.A. Scheidt, S.T. Nguyen, J.T. Hupp, Chem. Soc. Rev. 38 (2009) 1450.
[19] C.Y. Sun, S.X. Liu, D.D. Liang, K.Z. Shao, Y.H. Ren, Z.M. Su, J. Am. Chem. Soc. 131 (2009) 1883.
[20] X.S. Wang, S. Ma, D. Sun, S. Parkin, H.C. Zhou, J. Am. Chem. Soc. 128 (2006) 16474.
[21] C.C. Wang, H.P. Jing, P. Wang, J. Mol. Struct. 1074 (2014) 92.
[22] K. Sumida, D.L. Rogow, J.A. Mason, T.M. McDonald, E.D. Bloch, Z.R. Herm, T.H. Bae, J.R. Long, Chem. Rev. 112 (2011) 724.
[23] J.-R. Li, Y. Ma, M.C. McCarthy, J. Sculley, J. Yu, H.K. Jeong, P.B. Balbuena, H.C. Zhou, Coord. Chem. Rev. 255 (2011) 1791.
[24] A.R. Millward, O.M. Yaghi, J. Am. Chem. Soc. 127 (2005) 17998.
[25] J.M. Simmons, H. Wu, W. Zhou, T. Yildirim, Energy Environ. Sci. 4 (2011) 2177.
[26] C.C. Wang, P. Wang, L.I. Feng, Transit. Met. Chem. 37 (2012) 225.
[27] L.B. Sun, J.R. Li, W. Lu, Z.Y. Gu, Z. Luo, H.C. Zhou, J. Am. Chem. Soc. 134 (2012) 15923.
[28] Y. Xie, H. Yang, Z.U. Wang, Y. Liu, H.C. Zhou, J.R. Li, Chem. Commun. 50 (2014) 563.
[29] H.C. Zhou, J.R. Long, O.M. Yaghi, Chem. Rev. 112 (2012) 673.
[30] H. Lin, P.A. Maggard, Inorg. Chem. 47 (2008) 8044.
[31] Z.L. Liao, G.D. Li, M.H. Bi, J.S. Chen, Inorg. Chem. 47 (2008) 4844.
[32] Z.T. Yu, Z.L. Liao, Y.S. Jiang, G.H. Li, G.D. Li, J.S. Chen, Chem. Commun. (2004) 1814.
[33] Z.T. Yu, Z.L. Liao, Y.S. Jiang, G.H. Li, J.S. Chen, Chem. – Eur. J. 11 (2005) 2642.
[34] T. Toyao, M. Saito, Y. Horiuchi, K. Mochizuki, M. Iwata, H. Higashimura, M. Matsuoka, Catal. Sci. Technol. 3 (2013) 2092.
[35] C.G. Silva, A. Corma, H. García, J. Mater. Chem. 20 (2010) 3141.
[36] Y. Fu, D. Sun, Y. Chen, R. Huang, Z. Ding, X. Fu, Z. Li, Angew. Chem. 124 (2012) 3420.
[37] T. Zhou, Y. Du, A. Borgna, J. Hong, Y. Wang, J. Han, W. Zhang, R. Xu, Energy Environ. Sci. 6 (2013) 3229.
[38] Y. Horiuchi, T. Toyao, M. Saito, K. Mochizuki, M. Iwata, H. Higashimura, M. Anpo, M. Matsuoka, J. Phys. Chem. C 116 (2012) 20848.

[39] K.G. Laurier, F. Vermoortele, R. Ameloot, D.E. De Vos, J. Hofkens, M.B. Roeffaers, J. Am. Chem. Soc. 135 (2013) 14488.
[40] G.X. Liu, K. Zhu, H. Chen, R.Y. Huang, X.M. Ren, Z. Anorg. Allg. Chem. 635 (2009) 156.
[41] Bruker AXS, SMART, Version 5.611, Bruker AXS, Madison, WI, USA, 2000.
[42] Bruker AXS, SAINT, Version 6.28, Bruker AXS, Madison, WI, USA, 2003.
[43] SADABS, V2.03, Bruker AXS, Madison, WI, 2000.
[44] G.M. Sheldrick, SHELX-97, Göttingen University, Germany, 1997.
[45] W.Q. Kan, B. Liu, J. Yang, Y.Y. Liu, J.F. Ma, Cryst. Growth Des. 12 (2012) 2288.
[46] H.Y. Liu, L. Bo, J. Yang, Y.Y. Liu, J.F. Ma, H. Wu, Dalton Trans. 40 (2011) 9782.
[47] L. Zhou, C. Wang, X. Zheng, Z. Tian, L. Wen, H. Qu, D. Li, Dalton Trans. 42 (2013) 16375.
[48] X. Li, J. Li, M.K. Li, Z. Fei, J. Mol. Struct. 1059 (2014) 294.
[49] X.L. Wang, Y. Qu, G.C. Liu, J. Luan, H.Y. Lin, X.M. Kan, Inorg. Chim. Acta 412 (2014) 104.
[50] C.C. Wang, J.-R. Li, X.L. Lv, Y.q. Zhang, G. Guo, Energy Environ. Sci. 7 (2014) 2831.
[51] W. Wang, J. Yang, W.Q. Kan, J.F. Ma, CrystEngComm 15 (2013) 5844.
[52] C. Gomes Silva, I. Luz, F.X. Llabrés i Xamena, A. Corma, H. García, Chem. – Eur. J. 16 (2010) 11133.
[53] Q. Zhang, J.n.M. Shreeve, Angew. Chem. Int. Ed. 53 (2014) 2540.
[54] F.X. Llabrés i Xamena, A. Abad, A. Corma, H. Garcia, J. Catal. 250 (2007) 294.
[55] M. Nasalevich, M. van der Veen, F. Kapteijn, J. Gascon, CrystEngComm 16 (2014) 4919.
[56] H.A. Lopez, A. Dhakshinamoorthy, B. Ferrer, P. Atienzar, M. Alvaro, H. Garcia, J. Phys. Chem. C 115 (2011) 22200.